

# Geophysical Research Letters<sup>®</sup>

## RESEARCH LETTER

10.1029/2021GL095088

### Key Points:

- We simulate the biogeochemical properties of online Lagrangian particles in the Southern Ocean
- Ocean bathymetry plays a disproportionate role in bringing deep, carbon-rich water to the Southern Ocean surface
- All upwelled particles in the upper ocean exhibit relatively uniform pCO<sub>2</sub> and rates of carbon transformation, regardless of their origin

### Supporting Information:

Supporting Information may be found in the online version of this article.

### Correspondence to:

R. X. Brady,  
[riley.bradly@colorado.edu](mailto:riley.bradly@colorado.edu)




### Citation:

Brady, R. X., Maltrud, M. E., Wolfram, P. J., Drake, H. F., & Lovenduski, N. S. (2021). The influence of ocean topography on the upwelling of carbon in the Southern Ocean. *Geophysical Research Letters*, 48, e2021GL095088. <https://doi.org/10.1029/2021GL095088>

Received 7 JUL 2021

Accepted 22 SEP 2021

## The Influence of Ocean Topography on the Upwelling of Carbon in the Southern Ocean

Riley X. Brady<sup>1</sup> , Mathew E. Maltrud<sup>2</sup>, Phillip J. Wolfram<sup>2</sup>, Henri F. Drake<sup>3</sup> , and Nicole S. Lovenduski<sup>1</sup> 

<sup>1</sup>Department of Atmospheric and Oceanic Sciences and Institute of Arctic and Alpine Research, University of Colorado, Boulder, CO, USA, <sup>2</sup>Fluid Dynamics and Solid Mechanics (T-3), Los Alamos National Laboratory, Los Alamos, NM, USA, <sup>3</sup>MIT-WHOI Joint Program in Oceanography/Applied Ocean Science & Engineering, Cambridge, MA, USA

**Abstract** The physical circulation of the Southern Ocean sets the surface concentration and thus air-sea exchange of CO<sub>2</sub>. However, we have a limited understanding of the three-dimensional circulation that brings deep carbon-rich waters to the surface. Here, we introduce and analyze a novel high-resolution ocean model simulation with active biogeochemistry and online Lagrangian particle tracking. We focus our attention on a subset of particles with high dissolved inorganic carbon (DIC) that originate below 1,000 m and eventually upwell into the near-surface layer (upper 200 m). We find that 71% of the DIC-enriched water upwelling across 1,000 m is concentrated near topographic features, which occupy just 33% of the Antarctic Circumpolar Current. Once particles upwell to the near-surface layer, they exhibit relatively uniform pCO<sub>2</sub> levels and DIC decorrelation timescales, regardless of their origin. Our results show that Southern Ocean bathymetry plays a key role in delivering carbon-rich waters to the surface.

**Plain Language Summary** The Southern Ocean is the only place in the world where ocean currents circle the globe without hitting land. Here, some of the strongest winds on the planet force water to flow west-to-east around Antarctica and bring water from kilometers deep up to the surface. These waters have traversed the deep ocean for centuries, and in that time have gathered large stores of carbon from dead algae that rain down from above. When this water is brought to the surface, it expels its large store of carbon to the atmosphere. This process is important for the carbon cycle, but has not been extensively studied. Here, we use a new ocean model simulation that estimates ocean carbon and follows virtual floats that flow around the ocean and measure simulated carbon levels. We use the model to figure out how deep carbon in the Southern Ocean reaches the surface. We find that a large fraction of the carbon that is brought up from depth to the surface occurs in a relatively small fraction of the Southern Ocean, near places with mountains on the sea floor. Our study demonstrates that mountains on the sea floor have an influence on the global carbon cycle.

## 1. Introduction

The physical circulation of the Southern Ocean is paramount to its carbon cycling (e.g., Landschützer et al., 2015; Lovenduski et al., 2008; Lovenduski et al., 2013). The region is characterized by a meridional overturning circulation whose upwelling limb brings deep waters enriched in old, respired carbon (Mikaloff Fletcher et al., 2007) to the surface (e.g., Marshall & Speer, 2012; Morrison et al., 2015). Once this natural CO<sub>2</sub> is released to the atmosphere it influences the global carbon cycle and climate system (Gruber et al., 2009).

Substantial progress has been made in studying the Southern Ocean carbon cycle along the air-sea interface (see Gruber et al. (2019)), albeit through the lens of limited observations. Due to the region's harsh conditions, the majority of observations have been biased to the austral summer and to areas with frequent ship traversals that resupply Antarctic research stations (Munro et al., 2015). Autonomous ocean profiling floats have recently been outfitted with sensors to estimate biogeochemical quantities, such as ocean pH, from which the partial pressure of CO<sub>2</sub> (pCO<sub>2</sub>) and the air-sea CO<sub>2</sub> flux can be derived (Johnson et al., 2017). These floats have begun to fill the seasonal and spatial gaps in our record and suggest that there is much stronger outgassing of CO<sub>2</sub> occurring in the Southern Ocean than previously estimated (Bushinsky et al., 2019; Gray et al., 2018). The unaccounted-for outgassing is inferred from elevated surface ocean

pCO<sub>2</sub> measurements in the upwelling limb of the Antarctic Circumpolar Current (ACC), between the Polar Frontal Zone and seasonal sea ice edge (Gray et al., 2018). Factors contributing to carbon transport from depth remain a mystery and further investigation requires an analysis of the physical underpinnings that contribute to dissolved CO<sub>2</sub> concentrations in the Southern Ocean.

Previous studies using Lagrangian ocean simulations suggest that vigorous upwelling in the Southern Ocean is confined to a few key regions, rather than occurring in a broadband fashion across all longitudes of the ACC (Sallée et al., 2010; Tamsitt et al., 2017; Viglione & Thompson, 2016). These upwelling hot spots tend to occur downstream of topographic features. Due to the conservation of potential vorticity, topographic features steer the ACC equatorward, causing jets in the ACC to converge (Rintoul, 2018). This convergence steepens isopycnals and promotes stronger eddy activity downstream of the bathymetry, intensifying the local residual upwelling (Rintoul, 2018). Although other factors contribute to the spatial heterogeneity of ocean upwelling in the Southern Ocean, we focus on bathymetric upwelling in this study because of the emphasis in previous oceanographic literature on the bathymetry as a leading factor of driving asymmetries (Rintoul, 2018). While previous model-based Lagrangian studies illuminated zonal asymmetries in Southern Ocean upwelling (Sallée et al., 2010; Tamsitt et al., 2017; Viglione & Thompson, 2016), no Lagrangian study has assessed the biogeochemical signatures of upwelling hot spots or the upwelling pathways that fuel their biogeochemistry. Further, these studies were conducted with “offline” Lagrangian particles, where trajectories are calculated using time-averaged velocity output from an Eulerian simulation, which can introduce error relative to using instantaneous velocities from the model (Qin et al., 2014).

Here, we aim to build upon the findings of previous Lagrangian studies of upwelling in the Southern Ocean by introducing and analyzing a novel global high-resolution ocean model simulation with active biogeochemistry and online Lagrangian particle tracking (i.e., at model runtime) for reduced error. Our Lagrangian particles are outfitted with virtual “sensors” that record the time history of physical and biogeochemical tracers along their trajectories, which allows us to consider the upwelling of dissolved CO<sub>2</sub>. We view this problem from a three-dimensional perspective that follows transport pathways, aiming to better understand the deep origins of high-pCO<sub>2</sub> waters, the locations in which they upwell, and their potential for air-sea CO<sub>2</sub> exchange once they reach the upper 200 m, which we refer to as the “near-surface layer” in this paper. Here, we use Lagrangian analysis to understand how topography contributes to Southern Ocean CO<sub>2</sub> outgassing, a key driver of the global carbon cycle.

## 2. Methods

### 2.1. Model Configuration

Our primary modeling tool is the ocean and sea ice components of the Energy Exascale Earth System Model (E3SM); Golaz et al. (2019); Burrows et al. (2020), the Model for Prediction Across Scales Ocean (MPAS-O) and the Model for Prediction Across Scales Sea Ice (Ringler et al., 2013). Our simulation is forced by momentum, heat, and freshwater fluxes from the Coordinated Ocean-ice Reference Experiments II (CORE-II) interannual atmospheric forcing data set (Large & Yeager, 2009). The ocean model component also includes active biogeochemistry, which is based on the Biogeochemical Elemental Cycling (BEC) model (Moore et al., 2013).

We use an unstructured hexagonal mesh (Figure S1) with a horizontal resolution varying from 30 km at the equator to 10 km at the poles (Figure S2). In the latitude range of the ACC (50°S - 60°S), the horizontal resolution is an eddy-permitting 14.5 km (Figure S2). The model has 80 vertical levels with a vertical resolution varying from 2 m at the surface to 150 m at depth and uses a z-star coordinate system (Petersen et al., 2015).

The atmospheric CO<sub>2</sub> boundary condition in our simulation is a constant 360 ppm, chosen to align with the main collection period for biogeochemical observations used to initialize the simulation (Key et al., 2004). While this atmospheric CO<sub>2</sub> concentration is well above pre-industrial levels of ~270 ppm, we focus on the circulation of deep, natural (pre-industrial) carbon to the surface, rather than the small surface perturbation due to anthropogenic carbon. Further, we recognize that this upwelling of carbon would have consequences for air-sea CO<sub>2</sub> flux, but we avoid quantifying it directly in this study, since the constant atmospheric CO<sub>2</sub> levels prevent our model from capturing the seasonality and magnitude of air-sea CO<sub>2</sub> fluxes of the real world.

See the supporting information for more details on model parameterizations, the ocean biogeochemical model, and model initialization and spinup (Text S1).

## 2.2. Lagrangian Particle Tracking System

Following the model spinup, we seeded the global ocean with approximately 1 million Lagrangian particles using Lagrangian, in Situ, Global, High-Performance Particle Tracking (LIGHT), which was written specifically for MPAS-O (Wolfram et al., 2015). Particles were seeded at cell centers, with 15 particles linearly spread over the ocean depth of the given grid cell. In order to keep the simulation computationally feasible, we horizontally downsampled the cell seeding locations using algebraic multi-grid splitting from PyAMG (Olson & Schroder, 2018). This resulted in approximately 300,000 particles initialized south of 45°S, which induced effectively no additional computational cost to the simulation (Wolfram et al., 2015).

The governing equation used for particle advection is

$$\frac{d\mathbf{x}}{dt} = \mathbf{u}[\mathbf{x}(t), t], \quad (1)$$

where three-dimensional Eulerian velocities from MPAS-O ( $\mathbf{u}$ ) were interpolated to particle positions ( $\mathbf{x}$ ) using Wachspress interpolation (Gillette et al., 2012). Particle trajectories were integrated at model runtime using second-order Runge-Kutta (RK2) with two-hourly averages of the velocity fields, composed of the ten-minute model time steps. We use RK2 rather than RK4 due to its lower cost and comparable spatiotemporal accuracy demonstrated in an idealized case of a circular ocean basin (Wolfram et al., 2015).

Note that we only advect particles with velocities resolved by the model. In other words, we do not use any stochastic terms for subgrid-scale processes such as mixing and diffusion, consistent with other model Lagrangian particle studies (e.g., Drake et al., 2018; Tamsitt et al., 2017). In the ocean interior, trajectories are, on average, adiabatic (Tamsitt et al., 2018), and thus upwelling trajectories are not strongly affected by the vertical mixing parameterization (Tamsitt et al., 2017).

We simulated LIGHT particles for 17 years, which matches the 17-year mode of the transit time distribution for Circumpolar Deep Water to reach the Southern Ocean surface at this model resolution (Drake et al., 2018). Trajectories were saved to disk every two days, recording instantaneous  $x$ ,  $y$ , and  $z$  positions as well as instantaneous temperature, salinity, dissolved inorganic carbon (DIC), alkalinity,  $\text{PO}_4$ ,  $\text{NO}_3$ , and  $\text{SiO}_3$ . Tracers were similarly interpolated from cell centers to particle positions using Wachspress interpolation (Gillette et al., 2012). Quantities such as  $\text{pCO}_2$  and potential density ( $\sigma_\theta$ ) were then calculated diagnostically using the recorded tracer values. See Movie S1 for a demonstration of the Lagrangian advection of DIC at depth over the course of one model year.

## 2.3. Model Evaluation

Comprehensive validation of a CORE-II-forced MPAS-O simulation can be found in Petersen et al. (2019). They show that MPAS-O does a suitable job at replicating ocean currents, heat transport, sea ice coverage, sea surface temperature, and salinity. The high-resolution mesh used in this study is capable of replicating strongly eddying flows, such as the ACC (Petersen et al., 2019). We provide further evaluation of our MPAS-O simulation in the Supporting Information S1, focusing on horizontal transport of the ACC, mixed layer depth, and deep concentrations of DIC. In summary, our model finds general agreement in all three fields against observations, with relatively high pattern correlations and relatively low error within the ACC (Figures S3–S5).

## 3. History of an Upwelled Particle

We begin by introducing the reader to an example particle trajectory (Figure 1); this narrative puts the methodology section into practice and helps to frame the forthcoming results, which will divide particles into groups for ensemble analysis. The particular particle on which we focus is initialized just beneath 1,000 m in the central Pacific sector of the ACC (Figure 1). Its final deep upwelling across 1,000 m occurs just under two years into its transit, coinciding with shallow bathymetry in the Drake Passage (Figure 1a). Note that we

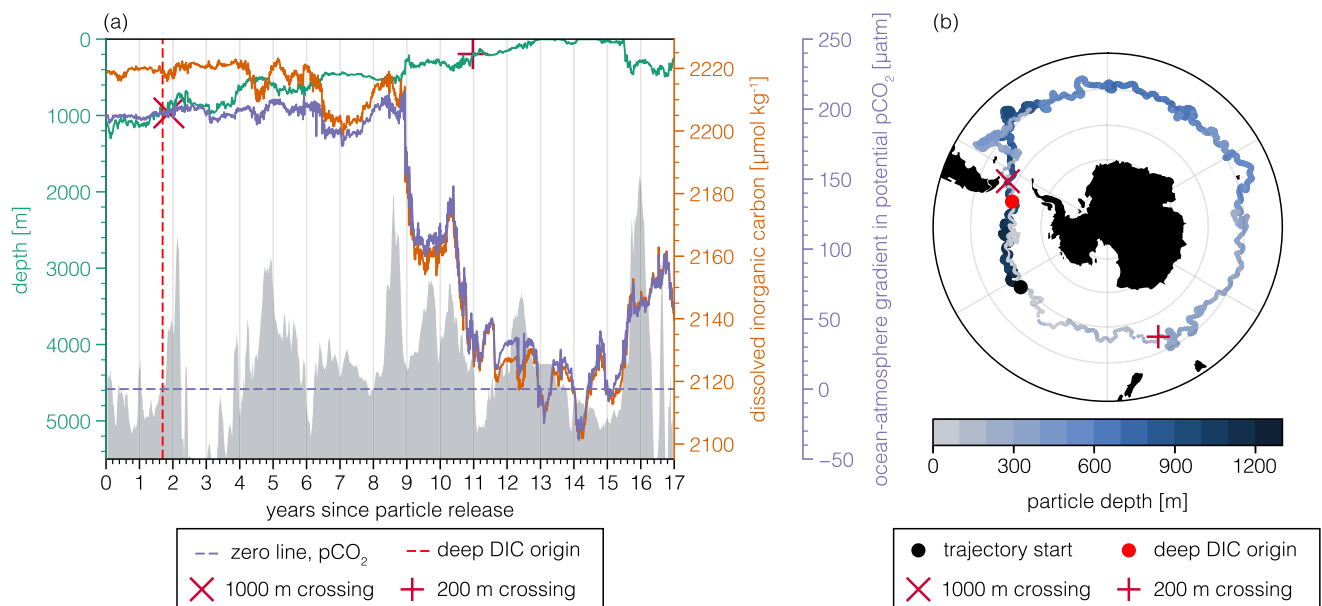


**Figure 1.** Tracer and location history of an upwelled particle in the Southern Ocean. (a) Depth (green), dissolved inorganic carbon (DIC) (orange), and the potential  $\text{pCO}_2$  gradient between the ocean and atmosphere (purple) over the 17-year particle history. The gray shading shows the ocean bathymetry from the nearest Eulerian grid cell and is smoothed over a 15-day centered rolling average. Potential  $\text{pCO}_2$  represents the  $\text{pCO}_2$  the particle would have if it were brought to 200 m without any circulation- or biology-driven changes and warmed or cooled to the ambient temperature at the location and time in which it crossed into 200 m (Sarmiento & Gruber, 2006). Potential  $\text{pCO}_2$  is subtracted by the fixed atmospheric  $\text{CO}_2$  concentration of  $360 \mu\text{atm}$ . Thus, when potential  $\text{pCO}_2$  is positive (above the purple dashed line), it would outgas carbon to the atmosphere. When negative (below the purple dashed line), it would uptake  $\text{CO}_2$  from the atmosphere. (b) Spatial history of the Lagrangian trajectory. The particle starts at the black dot in the Pacific sector and circumnavigates the Antarctic Circumpolar Current, ending near the Patagonian Shelf off of South America. The color of the trajectory denotes the particle depth and the thickness of the line is proportional to the concentration of DIC. The red “X” (in panels a and b) shows the first 1,000 m crossing of the particle and the red circle (red dashed line in panel a) shows the statistical source of DIC for the 1,000 m crossing. This source was computed using the  $e$ -folding decorrelation time scale (or “memory time”) of DIC prior to 1,000 m following Cetina-Heredia et al. (2018). The red “+” shows the subsequent 200 m crossing of the particle.

emphasize the final upwelling across 1,000 m to avoid statistical artifacts from particles that oscillate at high frequency around 1,000 m. The particle then circumnavigates the ACC with nearly monotonic upwelling, first crossing into 200 m near the Campbell Plateau (Figure 1). Upon entering the Drake Passage for a second time—around 15.5 years into its trajectory—the particle abruptly downwells and oscillates around a depth of approximately 350 m, ending its voyage in the Patagonian Shelf (Figure 1).

In order to statistically estimate the DIC source location of our example upwelled particle, we first calculate its “memory time” (Cetina-Heredia et al., 2018). The “memory time” represents the  $e$ -folding decorrelation timescale of DIC before the particle crosses 1,000 m (approximately 2 months for this particular particle). Following the particle’s trajectory backwards in time for two months, we find that the statistical origin of the particle’s DIC is about 650 km upstream of the Drake Passage (Figure 1b, red dot). This memory time analysis produces an unbiased estimate of the source of DIC for a given particle, and it does not require us to diagnose specific physical and biogeochemical processes.

Prior to upwelling into the near-surface layer, our example particle stores large amounts of carbon, averaging a DIC concentration of  $\sim 2220 \mu\text{mol kg}^{-1}$  and a potential  $\text{pCO}_2$  of  $\sim 560 \mu\text{atm}$ . This potential  $\text{pCO}_2$  is 200  $\mu\text{atm}$  higher than the atmosphere, which would lead to rapid outgassing of  $\text{CO}_2$  from the ocean. Potential  $\text{pCO}_2$  represents the  $\text{pCO}_2$  that the particle would have upon reaching 200 m, based on the ambient temperature at 200 m where and when the particle upwells, provided that there are no changes to DIC due to biology or circulation (Sarmiento & Gruber, 2006). Upon upwelling to 400 m depth just past the Kerguelen Plateau, the particle rapidly loses its carbon. Over the course of four months, the particle stays between 400 and 250 m depth and loses  $50 \mu\text{mol kg}^{-1}$  of DIC and  $90 \mu\text{atm}$  of potential  $\text{pCO}_2$ . The particle then upwells past 200 m and stays above this depth for nearly two years while traversing the Pacific Ocean between the Campbell Plateau and Drake Passage (Figure 1b). Here, surface processes such as photosynthesis and air-sea heat and gas exchange likely reduce the particle’s potential  $\text{pCO}_2$  enough for it to uptake  $\text{CO}_2$  from



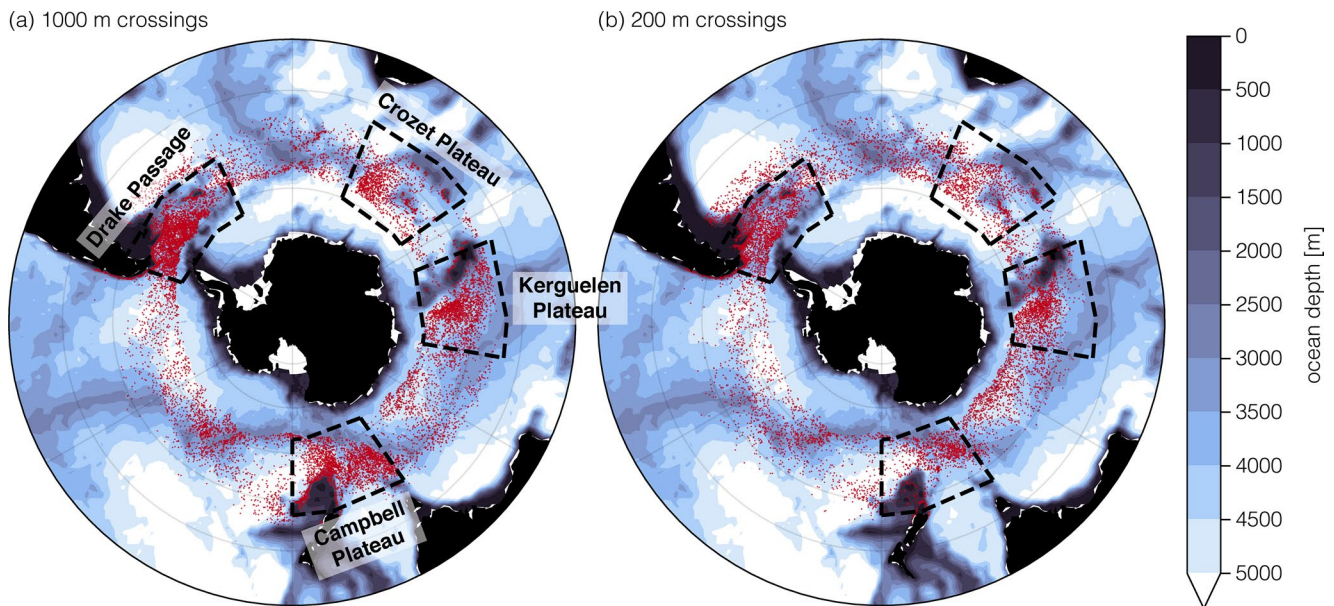


**Figure 2.** Upwelling locations of Lagrangian particles in the Antarctic Circumpolar Current (ACC). (a) 1,000 m upwelling locations that occurred in the ACC, south of  $45^{\circ}\text{S}$  and outside of the 75% annual sea ice zone. Only the final 1,000 m particle crossings during their 17-year trajectories are shown, and particles that do not ultimately reach 200 m are not included ( $N = 19,002$ ). Black dashed boxes show the four regions that are used for ensemble analysis, which are associated with topographic features and a disproportionate amount of upwelling relative to the region's surface area: the Drake Passage, Campbell Plateau, Kerguelen Plateau, and Crozet Plateau. (b) 200 m upwelling locations. Crossings are only shown for the particles from (a) whose first 200 m upwelling (following the 1,000 m crossing) occurred south of  $45^{\circ}\text{S}$  and outside of the 75% annual sea ice zone ( $N = 12,301$ ). Ocean bathymetry from the Eulerian model mesh is shown in purple contours.

the atmosphere during the austral summer and fall (December through April). Upon reaching the Drake Passage, the particle subducts between depths of 200 and 500 m.

The example particle trajectory outlined in this section demonstrates how we can apply statistical methods to our tracer time series to better understand the behavior of upwelled carbon in the Southern Ocean. We now turn to an ensemble view of particle trajectories to glean understanding of the bulk behavior of carbon upwelled in the Southern Ocean.

#### 4. Ensemble Analysis of Upwelled Carbon

Topographic features have a disproportionate influence on the upwelling of particles across both 1,000 m and 200 m in our simulation (Figure 2). Following Tamsitt et al. (2017), we organize particle trajectories into ensembles based on the location in which they last upwell across 1,000 m in the Southern Ocean. We ignore particles that upwell within the model's 75% annual sea ice extent to keep focus on upwelling occurring within the ACC. We further subset this by particles that ultimately reach at least 200 m before the simulation ends, to focus on particles that have an influence on near-surface layer properties. This results in a sample of 19,002 particles (Table 1).

We select four topographic regions that represent just 33% of the surface area of the ACC, but contribute to 71% of the total deep particle upwelling: the Drake Passage, Crozet Plateau, Kerguelen Plateau, and Campbell Plateau (Figure 2a; Table 1). These four regions are similar to those outlined in previous studies that identify the outsized influence of topography on Southern Ocean upwelling (Sallée et al., 2010; Tamsitt et al., 2017; Viglione & Thompson, 2016). We found that the selection of anomalous upwelling regions, and thus the relative percentages, are insensitive to the method used to define them (Figure S6). Roughly 65% of particles that upwell across 1,000 m within the ACC first reach 200 m within the ACC as well (Figure 2b). Of the remaining particles, 32% upwell into 200 m beneath the sea ice and 3% upwell into the near-surface layer north of  $45^{\circ}\text{S}$ . Note that we analyze the location in which particles first cross into the near-surface layer (after their last 1,000 m crossing), to assess where they initially influence and communicate with the upper

**Table 1***Geographic Information and Statistics for Deep (1,000 m) and Near-Surface Layer (200 m) Upwelled Particles That Occur Within and Outside of Topographic Regions in the Southern Ocean*

	Drake Passage	Crozet Plateau	Kerguelen Plateau	Campbell Plateau	Non-Topographic
<b>Geographic Information</b>					
Geographic coordinates	71°W – 25°W	22°E – 55°E	68°E – 100°E	145°E – 180°E	—
	63.4°S – 50°S	60°S – 45°S	60°S – 45°S	63°S – 47°S	—
% of ACC surface area	7.4%	8.1%	8.1%	9.2%	67.2%
<b>Deep Upwelling (1,000 m) Statistics</b>					
Number of particles	5,645	2,050	2,181	3,651	5,475
% of deep upwelled particles	29.7%	10.8%	11.5%	19.2%	28.8%
Zonal <sup>b</sup>	73.6°W ± 39.6° (4,740 km)	23.0°E ± 30.4° (4,150 km)	71.4°E ± 26.0° (3,690 km)	142.8°E ± 35.8° (4,910 km)	—
Meridional <sup>b</sup>	57.4°S ± 4.3° (950 km)	52.1°S ± 3.6° (800 km)	50.3°S ± 5.8° (1,280 km)	51.9°S ± 4.3° (960 km)	—
Median DIC memory time (days)	366	410	382	338	366
$\sigma_\theta$ of source waters [kg m <sup>-3</sup> ]	27.6 ± 0.2	27.6 ± 0.1	27.6 ± 0.1	27.5 ± 0.2	27.5 ± 0.2
DIC of source waters [ $\mu$ mol kg <sup>-1</sup> ]	2220 ± 23	2220 ± 15	2217 ± 13	2212 ± 21	2218 ± 21
Potential pCO <sub>2</sub> of source waters <sup>a</sup> [ $\mu$ atm]	486 ± 51	479 ± 33	481 ± 27	484 ± 51	482 ± 44
<b>Near-Surface Layer (200 m) Statistics</b>					
Number of particles <sup>a</sup>	3,104	1,646	1,632	1,393	4,526
% of upwelled particles	25.2%	13.4%	13.3%	11.3%	36.8%
decorrelation timescale of DIC (days)	44	44	44	42	40
residence time (days)	6	6	8	8	8

*Note.* All values including  $\pm$  indicate the median value  $\pm$  the standard deviation. Parentheses indicate the extent of  $-1\sigma$  to  $1\sigma$  in km. The decorrelation timescale of DIC above 200 m was calculated by assessing the  $e$ -folding time scale (i.e., the time at which the autocorrelation drops below  $1/e$ ) of every instance a particle from the given ensemble upwelled into 200 m, and the autocorrelation was statistically significant with  $p < 0.05$ . We also excluded 200 m crossings that occurred north of 45°S, within the 75% annual ice present zone, or within an ocean depth shallower than 500 m (to avoid coastally trapped particles). The residence time was computed alongside this calculation, and times were retained even in cases the particle did not decorrelate below  $\frac{1}{e}$  or when the decorrelation was not statistically significant.

<sup>a</sup>Particle ensembles are based on the location of their 200 m crossing, not their 1000 m crossing (as in Figure 2b). <sup>b</sup>Values are rounded to the nearest 10.

ocean and atmosphere. Although upwelling across 200 m is seemingly more spatially diffuse than across 1,000 m, our four regions that represent 33% of the surface area of the ACC contribute to 63% of the total near-surface layer particle upwelling (Figure 2a; Table 1). Thus, ocean topography has a disproportionate influence on upwelling of water both at deep (at 1,000 m) and shallow (at 200 m) depths.

Deep upwelled carbon is generally sourced from waters upstream of topographic features in a relatively narrow meridional band (Figure 3). Source waters of deep carbon span approximately 800–1,000 km meridionally, drawing primarily from the ACC region (Figure 3; Table 1). However, a notable exception over the regions we investigated is the Kerguelen Plateau, which draws DIC from subtropical waters originating in the Agulhas Return Current over 1,000 km away (Figure 3c). DIC source waters for deep upwelling vary much more zonally than meridionally between topographic regions (Table 1). The Campbell Plateau draws DIC from waters spanning a zonal range of 4,900 km—nearly one-quarter of the ACC (Figure 3d; Table 1). On the other hand, the Kerguelen Plateau DIC source originates from a much more narrow zonal band of 3,700 km (Figure 3c; Table 1). The Crozet Plateau and Drake Passage regions bring deep carbon from a zonal extent of 4,100 to 4,700 km (Figures 3a and 3b; Table 1).

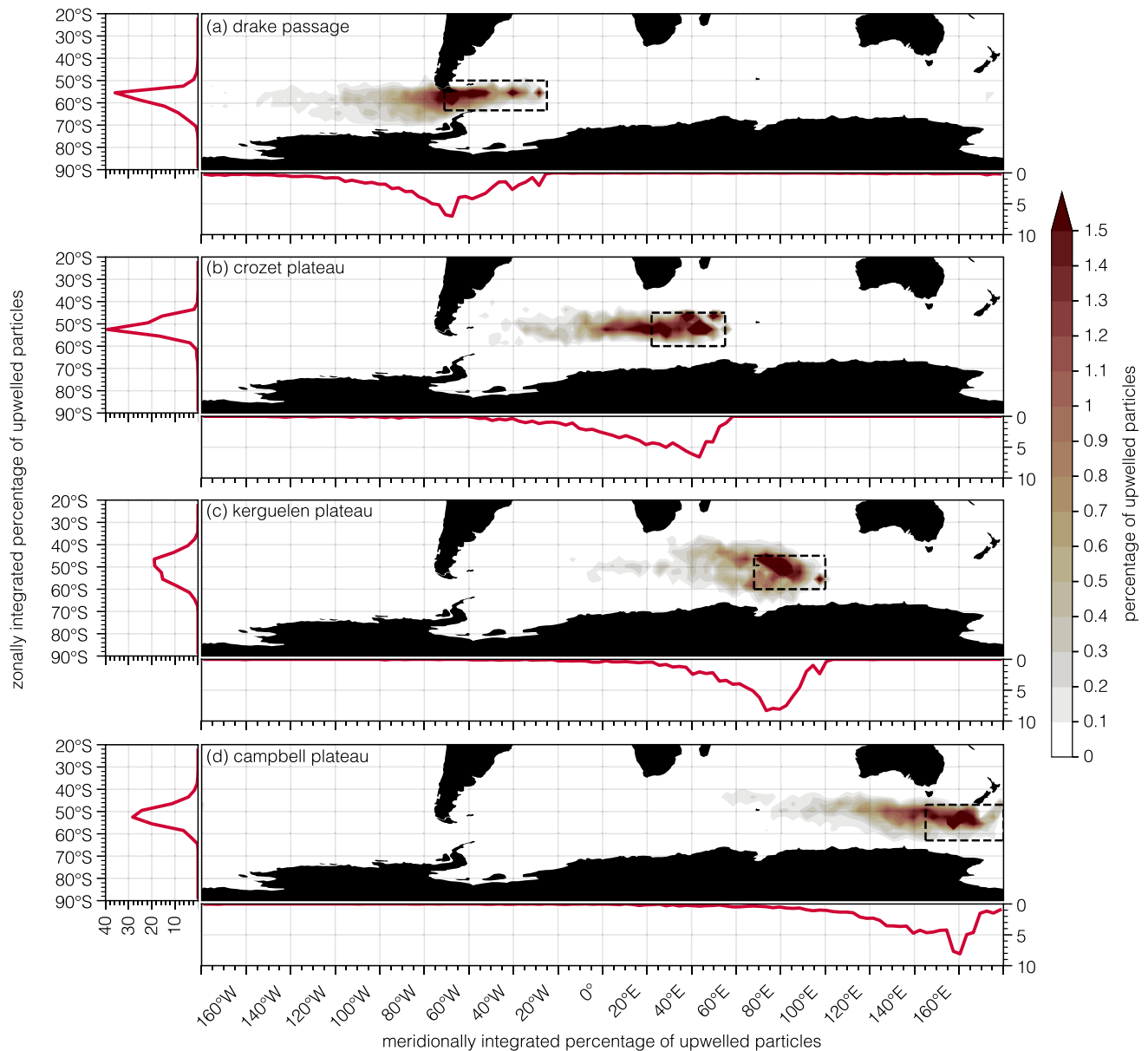


**Figure 3.** Statistical origin of deep (1,000 m) upwelled dissolved inorganic carbon for the four topographic regions. Particle ensembles were selected based on their final 1,000 m upwelling location (see Figure 2) and were subset based on the dashed boxes in (a–d). The maps in each panel show the memory time origin for each particle in the ensemble following Cetina-Heredia et al. (2018), based on the  $e$ -folding decorrelation time scale of the particle prior to its 1,000 m upwelling. The memory time ( $M$ ) is derived for each trajectory individually, and then the x-y coordinates are evaluated  $M$  time steps prior to the 1,000 m crossing. The side panels associated with each subplot show the zonal (left) and meridional (bottom) sum for each panel. All values are reported as the percentage of all particles in the given ensemble.

Circumpolar Deep Water (CDW) is the dominant source of DIC upwelling across 1,000 m in the topographically influenced regions (Figure 4a). However, Antarctic Intermediate Water (AAIW) also supplies a sizable portion of upwelled DIC in each of the regions. The Drake Passage (64%), Kerguelen Plateau (72.5%), and Crozet Plateau (86%) source a majority of their DIC from CDW, with the remainder attributed to the lighter AAIW (Figure 4a). The Campbell Plateau is a unique region, in that its sourced DIC is roughly split between CDW (46%) and AAIW (47.5%), with the remainder attributed to Subantarctic Mode Water (SAMW), Figure 4a. Despite the differences in water mass characteristics of source waters, all four regions upwell waters that are enriched with high concentrations of DIC and a large store of potential  $pCO_2$  relative to the atmosphere (Figures 4b and 4c; Table 1). Source water DIC varies in a narrow range of 2,212 to 2,220  $\mu\text{mol kg}^{-1}$

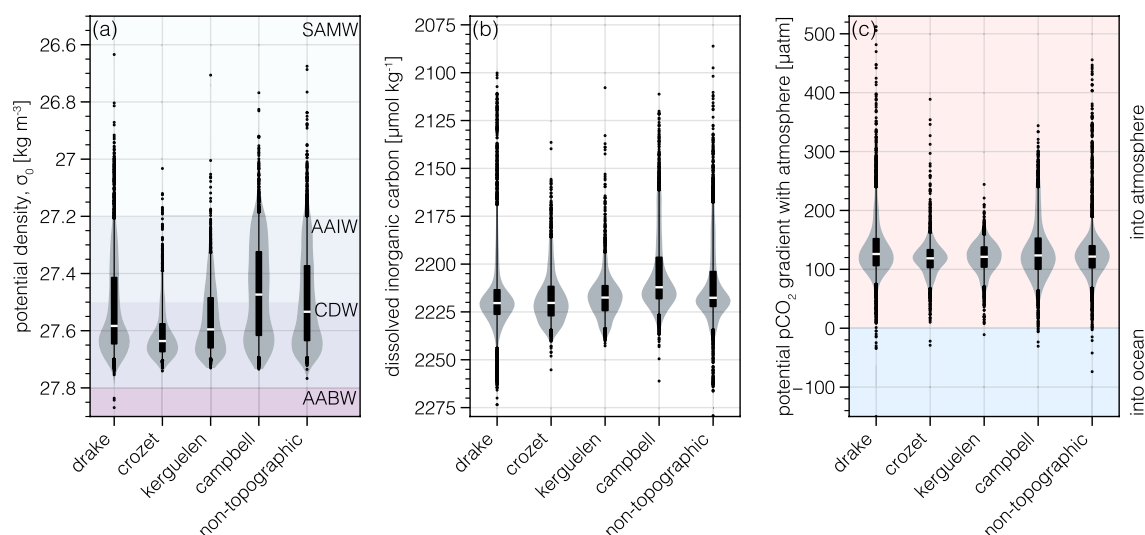


**Figure 4.** Properties of deep (1,000 m) upwelled waters in the Southern Ocean. Properties are based on the memory time ( $e$ -folding decorrelation time scale; Cetina-Heredia et al., 2018) for dissolved inorganic carbon (DIC) prior to upwelling across 1,000 m in the given topographic region. The memory time ( $M$ ) is derived for each trajectory individually, and then tracer concentrations are evaluated  $M$  time steps prior to the 1,000 m crossing. Boxes outline the 25% and 75% quantiles, with the white line showing the median. Whiskers outline the 5% and 95% quantiles, with black dots showing outliers (the remaining 10% of the data). The gray violin plots show the underlying distribution of the tracers. Each violin plot represents the ensemble of particles upwelling within the given topographic domain at 1,000 m, with the “non-topographic” region representing all particles upwelling at 1,000 m outside of the four defined regions. (a) DIC, (b) potential density (referenced to the surface), and (c) potential  $p\text{CO}_2$  minus the fixed atmospheric concentration of  $360 \mu\text{atm}$ . Potential  $p\text{CO}_2$  represents what the  $p\text{CO}_2$  concentration would be solely due to the thermal effects of bringing the particle from its current temperature to the ambient temperature when the given particle first upwells into 200 m (Sarmiento & Gruber, 2006). Water mass definitions are based on Schmitz (1996).

(Table 1). These carbon stores translate to waters with a strong outgassing potential. All four regions have a median potential  $p\text{CO}_2$  ranging from 130 to  $150 \mu\text{atm}$  higher than the fixed atmospheric concentration of  $360 \mu\text{atm}$ , and 99.9% of all source waters tend toward outgassing potential rather than uptake potential (Figure 4c; Table 1).

Upon reaching the near-surface layer, the DIC transformation on the particles is generally similar, regardless of the deep upwelling pathway taken by the particle. On average, all particles entering the near-surface layer have a DIC decorrelation time scale of 1.5 months (Table 1). The average residence time in the near-surface layer is approximately one week (Table 1), suggesting that DIC does not fully equilibrate with the atmosphere during the average single stay in the near-surface layer (Ito & Follows, 2013).

## 5. Conclusions & Discussion

We generated and analyzed a novel high-resolution simulation of a global ocean model with biogeochemistry and online Lagrangian particle tracking to illuminate the pathways over which natural carbon upwells from depth in the Southern Ocean. Our particles were equipped with virtual “sensors” to record physical and biogeochemical properties along their trajectories. We found that ocean topography plays a key role in bringing carbon-enriched waters to the surface; using the upwelling particle distribution, we selected four regions with prominent topographic features that cover just one-third of the ACC, but are responsible for 71% of particle upwelling across 1,000 m (Figure 2a; Table 1). All deep waters are enriched in DIC and have a high potential  $p\text{CO}_2$  relative to the atmosphere (Figures 4b and 4c; Table 1). Topographic regions create zonal asymmetries in the meridional overturning of the Southern Ocean and act as a conduit for circulating this relatively uniform deep carbon supply to the surface. After reaching the near-surface layer, the DIC behavior of upwelled particles are indistinguishable from one another, regardless of the particle’s origin (Figures 4b and 4c; Table 1). Our Lagrangian model analysis thus demonstrates that topographic features in the Southern Ocean bring disproportionately large quantities of the relatively uniform deep carbon stores to the surface, consistent with previous Eulerian analyses (Dufour et al., 2015). Further, our results indicate that the near-surface layer residence time of particles is an order of magnitude shorter than the decorrelation



time scale of DIC at the surface (Table 1). Particles remain above 200 m for roughly one week on average, but it takes 1.5 months for DIC to decorrelate (Table 1).

While this study presents a novel perspective on the three-dimensional circulation of carbon in the Southern Ocean, there are some caveats worth noting. First, our Lagrangian particle trajectories are only influenced by resolved advection, that is, we do not include any stochastic terms to simulate diffusion and unresolved physics (Van Sebille et al., 2018), and this could affect our estimates of near-surface layer residence times. However, our mesh has a horizontal resolution of ~14.5 km in the ACC (Figure S2) and thus resolves the influence of mesoscale eddies on trajectories. Further, upwelling in the Southern Ocean follows nearly adiabatic pathways prior to reaching the near-surface layer (Marshall & Speer, 2012). Second, we rely upon the accuracy of a single physical and biogeochemical model (MPAS-O and BEC) for our Lagrangian particle tracking system, which is biased relative to real world dynamics and biogeochemistry. However, our model evaluation and previous studies demonstrate that MPAS-O is suitable for simulating the circulation and sub-surface DIC concentrations of the Southern Ocean (Figures S3–S5; Petersen et al. (2019)). Third, our particle trajectories span 17 years, so we do not resolve the long tail of the transit time distribution for deep upwelling to the Southern Ocean surface (Drake et al., 2018). However, we do permit the mode of the transit time distribution (17 years), so our analysis likely includes the most representative trajectories (Drake et al., 2018). Our study required the use of a high-resolution horizontal mesh so that we could resolve mesoscale eddies and thus investigate the influence of topographic features on upwelling, which act to modify the eddy-driven component of Southern Ocean overturning (Rintoul, 2018). The temporal extent of our particle trajectories was limited because of computational expense. Finally, we did not explore particles that upwelled under sea ice. Sea ice caps surface waters from the atmosphere, and potentially reduces air-sea gas exchange (Gupta et al., 2020). Since the bulk of upwelling and air-sea gas exchange occurs in the core of the ACC, we focus our analysis there.

Our study builds upon work done by Viglione and Thompson (2016) and Tamsitt et al. (2017) by connecting the zonal asymmetries in physical circulation to the marine carbon cycle. To our knowledge, our study marks the first global high-resolution ocean biogeochemistry experiment with online Lagrangian particle tracking. Our results showcase the fine-grained analysis that can be performed with a Lagrangian perspective of ocean biogeochemistry by tracing out the pathways over which carbon circulates in the Southern Ocean. Our work further supports previous work by Ito and Follows (2013) that addresses the short residence time of water in the surface of the Southern Ocean relative to the air-sea CO<sub>2</sub> flux exchange time scale. There exists a tremendous amount of untapped biogeochemical information for future Lagrangian biogeochemical studies to reveal. Future studies could, for example, focus on the behavior of carbon upwelled under sea ice. Further, an analysis similar to this could be conducted in many other regions of the world oceans, where carbon and other biogeochemical tracer pathways are under intense study (e.g., the California Current; Rykaczewski & Dunne, 2010; Pozo Buil & Di Lorenzo, 2017). While the computational expense of a high-resolution global online Lagrangian study is high, the insights gleaned from such a simulation are invaluable. In this case, we have found that seamounts and ridges on the Southern Ocean seafloor ultimately dictate the three-dimensional movement of deep carbon to the ocean's surface and have the potential to influence air-sea CO<sub>2</sub> exchange.

#### Acknowledgments

Riley X. Brady was supported by the Department of Energy's Computational Science Graduate Fellowship (DE-FG02-97ER25308), and particularly benefited from the fellowship's summer practicum at Los Alamos National Lab. Nicole S. Lovenduski and Riley X. Brady were further supported by the U.S. Department of Energy Biological and Environmental Research program (DE-SC0022243) and by the National Science Foundation (NSF-PLR 1543457; NSF-OCE 1924636; NSF-OCE 1752724; NSF-OCE 1558225). Mathew E. Maltrud and Phillip J. Wolfram were supported as part of the Energy Exascale Earth System Model (E3SM) project, funded by the U.S. Department of Energy, Office of Science, Office of Biological and Environmental Research. This research used resources provided by the Los Alamos National Laboratory Institutional Computing Program, which is supported by the U.S. Department of Energy National Nuclear Security Administration under Contract No. 89233218CNA000001. The Climate, Ocean and Sea Ice Modeling (COSIM) team at LANL provided invaluable feedback and support during the project.

#### Data Availability Statement

The Lagrangian particle output used in this study and the code used to generate the main figures and table in the text can be found on Zenodo at <https://zenodo.org/record/4281539>, <https://doi.org/10.5281/zenodo.4281539>.

#### References

- Burrows, S., Maltrud, M., Yang, X., Zhu, Q., Jeffery, N., Shi, X., et al. (2020). The DOE E3SM v1. 1 biogeochemistry configuration: Description and simulated ecosystem-climate responses to historical changes in forcing. *Journal of Advances in Modeling Earth Systems*, 12(9), e2019MS001766. <https://doi.org/10.1029/2019MS001766>
- Bushinsky, S. M., Landschützer, P., Rödenbeck, C., Gray, A. R., Baker, D., Mazloff, M. R., et al. (2019). Reassessing Southern Ocean air-sea CO<sub>2</sub> flux estimates with the addition of biogeochemical float observations. *Global Biogeochemical Cycles*, 33(11), 1370–1388. <https://doi.org/10.1029/2019gb006176>

- Cetina-Heredia, P., van Sebille, E., Matear, R. J., & Roughan, M. (2018). Nitrate sources, supply, and phytoplankton growth in the Great Australian Bight: An Eulerian-Lagrangian modeling approach. *Journal of Geophysical Research: Oceans*, 123(2), 759–772. <https://doi.org/10.1002/2017JC013542>
- Drake, H. F., Morrison, A. K., Griffies, S. M., Sarmiento, J. L., Weijer, W., & Gray, A. R. (2018). Lagrangian timescales of Southern Ocean upwelling in a hierarchy of model resolutions. *Geophysical Research Letters*, 45(2), 891–898. <https://doi.org/10.1002/2017gl076045>
- Dufour, C. O., Griffies, S. M., de Souza, G. F., Frenger, I., Morrison, A. K., Palter, J. B., et al. (2015). Role of mesoscale eddies in cross-frontal transport of heat and biogeochemical tracers in the Southern Ocean. *Journal of Physical Oceanography*, 45(12), 3057–3081. <https://doi.org/10.1175/jpo-d-14-0240.1>
- Gillette, A., Rand, A., & Bajaj, C. (2012). Error estimates for generalized barycentric interpolation. *Advances in Computational Mathematics*, 37(3), 417–439. <https://doi.org/10.1007/s10444-011-9218-z>
- Golaz, J.-C., Caldwell, P. M., Van Roekel, L. P., Petersen, M. R., Tang, Q., Wolfe, J. D., et al. (2019). The DOE E3SM coupled model version 1: Overview and evaluation at standard resolution. *Journal of Advances in Modeling Earth Systems*, 11(7), 2089–2129. <https://doi.org/10.1029/2018MS001603>
- Gray, A. R., Johnson, K. S., Bushinsky, S. M., Riser, S. C., Russell, J. L., Talley, L. D., et al. (2018). Autonomous biogeochemical floats detect significant carbon dioxide outgassing in the high-latitude Southern Ocean. *Geophysical Research Letters*, 45(17), 9049–9057. <https://doi.org/10.1029/2018gl078013>
- Gruber, N., Gloor, M., Mikaloff Fletcher, S. E., Doney, S. C., Dutkiewicz, S., Follows, M. J., et al. (2009). Oceanic sources, sinks, and transport of atmospheric CO<sub>2</sub>. *Global Biogeochemical Cycles*, 23(1). <https://doi.org/10.1029/2008gb003349>
- Gruber, N., Landschützer, P., & Lovenduski, N. S. (2019). The variable Southern Ocean carbon sink. *Annual review of marine science*, 11, 159–186. <https://doi.org/10.1146/annurev-marine-121916-063407>
- Gupta, M., Follows, M. J., & Lauderdale, J. M. (2020). The effect of Antarctic sea ice on Southern Ocean carbon outgassing: Capping versus light attenuation. *Global Biogeochemical Cycles*, 34(8), e2019GB006489. <https://doi.org/10.1029/2019gb006489>
- Ito, T., & Follows, M. J. (2013). Air-sea disequilibrium of carbon dioxide enhances the biological carbon sequestration in the Southern Ocean. *Global Biogeochemical Cycles*, 27(4), 1129–1138. <https://doi.org/10.1002/2013gb004682>
- Johnson, K. S., Plant, J. N., Coletti, L. J., Jannasch, H. W., Sakamoto, C. M., Riser, S. C., Swift, D. D., et al. (2017). Biogeochemical sensor performance in the SOCCOM profiling float array. *Journal of Geophysical Research: Oceans*, 122(8), 6416–6436. <https://doi.org/10.1002/2017jc012838>
- Key, R. M., Kozyr, A., Sabine, C. L., Lee, K., Wanninkhof, R., Bullister, J. L., & Peng, T.-H. (2004). A global ocean carbon climatology: Results from Global Data Analysis Project (GLODAP). *Global Biogeochemical Cycles*, 18(4). <https://doi.org/10.1029/2004gb002247>
- Landschützer, P., Gruber, N., Haumann, F. A., Rödenbeck, C., Bakker, D. C., Van Heuven, S., et al. (2015). The reinvigoration of the Southern Ocean carbon sink. *Science*, 349(6253), 1221–1224. <https://doi.org/10.1126/science.aab2620>
- Large, W., & Yeager, S. (2009). The global climatology of an interannually varying air–sea flux data set. *Climate Dynamics*, 33(2–3), 341–364. <https://doi.org/10.1007/s00382-008-0441-3>
- Lovenduski, N. S., Gruber, N., & Doney, S. C. (2008). Toward a mechanistic understanding of the decadal trends in the Southern Ocean carbon sink. *Global Biogeochemical Cycles*, 22(3). <https://doi.org/10.1029/2007gb003139>
- Lovenduski, N. S., Long, M. C., Gent, P. R., & Lindsay, K. (2013). Multi-decadal trends in the advection and mixing of natural carbon in the Southern Ocean. *Geophysical Research Letters*, 40(1), 139–142. <https://doi.org/10.1029/2012gl054483>
- Marshall, J., & Speer, K. (2012). Closure of the meridional overturning circulation through Southern Ocean upwelling. *Nature Geoscience*, 5(3), 171–180. <https://doi.org/10.1038/ngeo1391>
- Mikaloff Fletcher, S., Gruber, N., Jacobson, A. R., Gloor, M., Doney, S., Dutkiewicz, S., et al. (2007). Inverse estimates of the oceanic sources and sinks of natural CO<sub>2</sub> and the implied oceanic carbon transport. *Global Biogeochemical Cycles*, 21(1), GB1010. <https://doi.org/10.1029/2006gb002751>
- Moore, J. K., Lindsay, K., Doney, S. C., Long, M. C., & Misumi, K. (2013). Marine ecosystem dynamics and biogeochemical cycling in the Community Earth System Model [CESM1 (BGC)]: Comparison of the 1990s with the 2090s under the RCP4.5 and RCP8.5 scenarios. *Journal of Climate*, 26(23), 9291–9312. <https://doi.org/10.1175/jcli-d-12-00566.1>
- Morrison, A. K., Frölicher, T. L., & Sarmiento, J. L. (2015). Upwelling in the Southern Ocean. *Physics Today*, 68(1), 27–32. <https://doi.org/10.1063/pt.3.2654>
- Munro, D. R., Lovenduski, N. S., Takahashi, T., Stephens, B. B., Newberger, T., & Sweeney, C. (2015). Recent evidence for a strengthening CO<sub>2</sub> sink in the Southern Ocean from carbonate system measurements in the Drake Passage (2002–2015). *Geophysical Research Letters*, 42(18), 7623–7630. <https://doi.org/10.1002/2015gl065194>
- Olson, L. N., & Schroder, J. B. (2018). PyAMG: Algebraic multigrid solvers in Python v4.0. (Release 4.0). Retrieved from <https://github.com/pyamg/pyamg>
- Petersen, M. R., Asay-Davis, X. S., Berres, A. S., Chen, Q., Feige, N., Hoffman, M. J., et al. (2019). An evaluation of the ocean and sea ice climate of E3SM using MPAS and interannual CORE-II forcing. *Journal of Advances in Modeling Earth Systems*, 11(5), 1438–1458. <https://doi.org/10.1029/2018ms001373>
- Petersen, M. R., Jacobsen, D. W., Ringler, T. D., Hecht, M. W., & Maltrud, M. E. (2015). Evaluation of the arbitrary Lagrangian–Eulerian vertical coordinate method in the MPAS–Ocean model. *Ocean Modelling*, 86, 93–113. <https://doi.org/10.1016/j.ocemod.2014.12.004>
- Pozo Buil, M., & Di Lorenzo, E. (2017). Decadal dynamics and predictability of oxygen and subsurface tracers in the California Current System. *Geophysical Research Letters*, 44(9), 4204–4213. <https://doi.org/10.1002/2017gl072931>
- Qin, X., van Sebille, E., & Gupta, A. S. (2014). Quantification of errors induced by temporal resolution on Lagrangian particles in an eddy-resolving model. *Ocean Modelling*, 76, 20–30. <https://doi.org/10.1016/j.ocemod.2014.02.002>
- Ringler, T., Petersen, M., Higdon, R. L., Jacobsen, D., Jones, P. W., & Maltrud, M. (2013). A multi-resolution approach to global ocean modeling. *Ocean Modelling*, 69, 211–232. <https://doi.org/10.1016/j.ocemod.2013.04.010>
- Rintoul, S. R. (2018). The global influence of localized dynamics in the Southern Ocean. *Nature*, 558(7709), 209–218. <https://doi.org/10.1038/s41586-018-0182-3>
- Rykaczewski, R. R., & Dunne, J. P. (2010). Enhanced nutrient supply to the California Current ecosystem with global warming and increased stratification in an Earth system model. *Geophysical Research Letters*, 37(21), L21606. <https://doi.org/10.1029/2010gl045019>
- Sallée, J.-B., Speer, K., Rintoul, S., & Wijffels, S. (2010). Southern Ocean thermocline ventilation. *Journal of Physical Oceanography*, 40(3), 509–529. <https://doi.org/10.1175/2009jpo4291.1>
- Sarmiento, J. L., & Gruber, N. (2006). *Ocean biogeochemical dynamics*. Princeton University Press.
- Schmitz, W. J. (1996). On the world ocean circulation. Volume II: The Pacific and Indian oceans—A global update. *Tech. Rep. WHOI-96-08*, 241.

- Tamsitt, V., Abernathey, R., Mazloff, M., Wang, J., & Talley, L. (2018). Transformation of deep water masses along Lagrangian upwelling pathways in the Southern Ocean. *Journal of Geophysical Research: Oceans*, 123(3), 1994–2017. <https://doi.org/10.1002/2017jc013409>
- Tamsitt, V., Drake, H. F., Morrison, A. K., Talley, L. D., Dufour, C. O., Gray, A. R., et al. (2017). Spiraling pathways of global deep waters to the surface of the Southern Ocean. *Nature Communications*, 8(1), 1–10. <https://doi.org/10.1038/s41467-017-00197-0>
- Van Sebillie, E., Griffies, S. M., Abernathey, R., Adams, T. P., Berloff, P., Biastoch, A., et al. (2018). Lagrangian ocean analysis: Fundamentals and practices. *Ocean Modelling*, 121, 49–75. <https://doi.org/10.1016/j.ocemod.2017.11.008>
- Viglione, G. A., & Thompson, A. F. (2016). Lagrangian pathways of upwelling in the Southern Ocean. *Journal of Geophysical Research: Oceans*, 121(8), 6295–6309. <https://doi.org/10.1002/2016jc011773>
- Wolfram, P. J., Ringler, T. D., Maltrud, M. E., Jacobsen, D. W., & Petersen, M. R. (2015). Diagnosing isopycnal diffusivity in an eddying, idealized midlatitude ocean basin via Lagrangian, in situ, global, high-performance particle tracking (LIGHT). *Journal of Physical Oceanography*, 45(8), 2114–2133. <https://doi.org/10.1175/jpo-d-14-0260.1>

## References From the Supporting Information

- Garcia, H. E., Locarnini, R. A., Boyer, T. P., Antonov, J. I., Baranova, O. K., Zweng, M. M., & Levitus, S. (2013). *World Ocean Atlas 2013. volume 4, dissolved inorganic nutrients (phosphate, nitrate, silicate)*.
- Holte, J., Talley, L. D., Gilson, J., & Roemmich, D. (2017). An argo mixed layer climatology and database. *Geophysical Research Letters*, 44(11), 5618–5626. <https://doi.org/10.1002/2017GL073426>
- Large, W. G., McWilliams, J. C., & Doney, S. C. (1994). Oceanic vertical mixing: A review and a model with a nonlocal boundary layer parameterization. *Reviews of Geophysics*, 32(4), 363–403. <https://doi.org/10.1029/94RG01872>
- Mazloff, M. R., Heimbach, P., & Wunsch, C. (2010). An eddy-permitting Southern Ocean state estimate. *Journal of Physical Oceanography*, 40(5), 880–899. <https://doi.org/10.1175/2009JPO4236.1>
- Wang, S., & Moore, J. K. (2011). Incorporating Phaeocystis into a Southern Ocean ecosystem model. *Journal of Geophysical Research: Oceans*, 116(C1), C01019. <https://doi.org/10.1029/2009JC005817>
- Zanowski, H., Hallberg, R., & Sarmiento, J. L. (2015). Abyssal ocean warming and salinification after Weddell polynyas in the GFDL CM2G coupled climate model. *Journal of Physical Oceanography*, 45(11), 2755–2772. <https://doi.org/10.1175/JPO-D-15-0109.1>